V. V. Filchenkov, N. N. Grafov, K. I. Gritsaj

INFLUENCE OF THE EPITHERMAL EFFECTS
ON THE MCF STEADY STATE

Работа посвящена проблеме корректной интерпретации параметров стационарного режима процесса мюонного катализа (МК) в смеси D/T. Ранее влияние *эпитермальных* эффектов (образование молекул $dt\mu$ «горячими», нетермализованными атомами $t\mu$) на параметры стационарного режима было изучено только для измерений с мишенями малой плотности (плотность $\varphi = 0,01$ относительно плотности жидкого водорода). Мы предлагаем новый метод, позволяющий прямое определение необходимых поправок к скорости цикла МК для данных высокой плотности ($\varphi \geq 0.4$).

Работа выполнена в Лаборатории ядерных проблем им. В. П. Джелепова ОИЯИ.

This work is devoted to the correct interpretation of the steady-state parameters of the muon catalyzed fusion (MCF) process in a D/T mixture. Previously the influence of the *epithermal* effects ($dt\mu$-molecule formation by «hot», non-thermalized $t\mu$ atoms) on the steady-state parameters was studied only for measurements with a low-density target (density $\varphi = 0.01$ relative to the liquid hydrogen density). We suggest a new method allowing direct determination of the necessary corrections to the MCF cycling rate for high-density data ($\varphi \geq 0.4$).

The investigation has been performed at the Dzelepov Laboratory of Nuclear Problems, JINR.

INTRODUCTION

In the MCF investigations one often deals with the fast transition stage for which the muonic molecule formation rate is much higher than for the steady state. An excellent example of this is the $d + d$ MCF reaction at low deuterium temperatures where the $dd\mu$-molecule formation rate for the rapidly degrading upper $d\mu$-atom spin state is at least an order of magnitude higher than for the lower one.

In the MCF $d + t$ reaction

$$t\mu + d \longrightarrow dt\mu \longrightarrow {}^4\text{He}(3.5\,\text{MeV}) + n(14.1\,\text{MeV}) + \mu \tag{1}$$
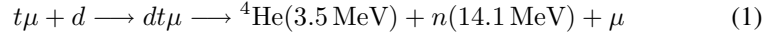
the fast stage is caused by passage of $t\mu$ atoms through intensive resonances of muonic molecule formation in the process of thermalization. Corrections to the steady-state parameters caused by the epithermal effects should be taken into account for the correct comparison between experiment and theory.

As follows from the «standard» theory [1, 2] the $dt\mu$-molecule formation in the interactions of $t\mu$-atoms with D_2, DT or HD molecules has a resonance (on the $t\mu$ atom kinetic energy) character. The main resonances are shown in Fig. 1 (taken from [2]).
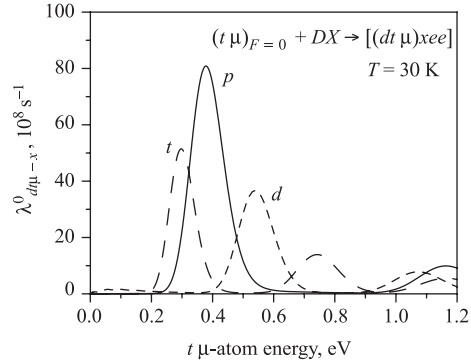

Fig. 1. The $dt\mu$-molecule formation rates for the $t\mu$-atom spin $F = 0$ and temperature $T = 30$ K on D_2 ($x = d$, $X = D$), DT ($x = t$, $X = T$) and HD ($x = p$, $X = H$) molecules [2]

As is seen from the figure, the resonances are placed at $t\mu$-atom energies $E_{t\mu} > 0.2$ eV that is higher than Maxwell distributed energies for «usual» temperatures ($T \leq 300$ K). Really, only for $T \geq 300$ K the Maxwell distribution begins to overlap the nearest resonance (on DT molecules).

At the lowest temperatures intensive $dt\mu$-molecule formation takes place not by the «standard» Vesman scheme but by the exotic three-particle mechanism on the «negative» resonance $t\mu + D_2$ where the energy excess is carried away by the third particle [3]. This process turns out to be strongly dependent on density. This is illustrated in Fig. 2, where the $dt\mu$-molecule formation rates on D_2 ($\lambda_{dt\mu-d}$) and DT ($\lambda_{dt\mu-t}$) are shown as a function of density (φ) and temperature (taken from [4]).
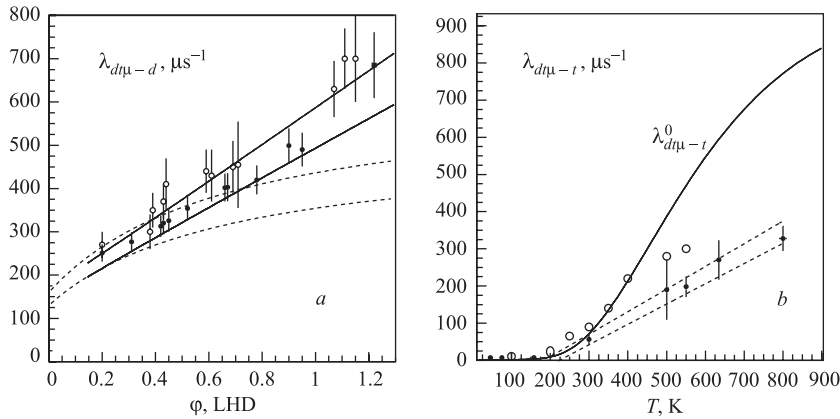

Fig. 2. *a*) $\lambda_{dt\mu-d}$ as a function of density for $T \leq 300$ K. Filled circles are our points for gas [4], empty circles are the results of LAMPF [5], the square is the result of paper [4] for liquid. Solid lines are the permissible values found from fit [4]. Dashed lines are limits for the $\lambda_{dt\mu-d}$ region obtained in [6]. *b*) $\lambda_{dt\mu-t}$ as a function of temperature. Filled circles are our points [4], empty circles are the results of LAMPF [5]. The solid line is the theory [2] for $\lambda^0_{dt\mu-t}$. Dashed lines are limits of parametrization [4]. All data are reduced to the liquid hydrogen density (LHD $= 4.25 \cdot 10^{22}$ nuclei/cm^3)

If the $t\mu$ atom is formed due to the transfer process $d\mu + t \rightarrow t\mu + d$ it acquires the energy 19 eV. There is no confident data on the energy distribution of the directly formed $t\mu$ atoms. It is accepted that they are distributed around the mean energy 1–2 eV. In any case, the energetic («hot») $t\mu$ atoms first pass through the resonance and then are thermalized. The thermalization rate is much higher than the muon disappearance

$$\lambda_0 = 0.455 \, \mu\text{s}^{-1}.$$

2

So, the MCF process in D/T mixture can be divided in two stages: «fast» and «slow» (steady state). As follows from Figs. 1, 2, the $dt\mu$-molecule formation rate for the steady state $\lambda_{dt\mu}^s$ is much lower than the rate $\lambda_{dt\mu}^f$ directly related to the resonances.

The experimentally measured parameter which determines the dynamics of the MCF process is cycling rate λ_c (mean reversal time between the MCF cycles). It is determined not only by $\lambda_{dt\mu}$ but by the rate of transition $d\mu + t \rightarrow t\mu + d$ also. The expression for λ_c has the form

$$\frac{1}{\lambda_c} \simeq \frac{q_{1s} \cdot C_d}{\lambda_{dt} \cdot C_t} + \frac{0.75}{\lambda_{1-0}C_t} + \frac{1}{\lambda_{dt\mu-d} \cdot C_{DD} + \lambda_{dt\mu-t} \cdot C_{DT}}, \qquad (2)$$

where C_x, C_{XX} $(x = d, t, X = D, T)$ are isotope and molecular mixture concentrations; q_{1S} is the fraction of $d\mu$ atoms in the ground state after muon cascade processes; λ_{1-0} is the $t\mu$-atom spin-flip rate and λ_{dt} is the rate of muon transfer $d\mu \rightarrow t\mu$ from the ground state of $d\mu$ atom.

The values $\lambda_{dt\mu-d}$ and $\lambda_{dt\mu-t}$ are extracted from the dependence $\lambda_c(C_t)$ given by Eq. (2). The examples of such dependences measured at temperature $T = 160$ K and at different densities are presented in Fig. 3.
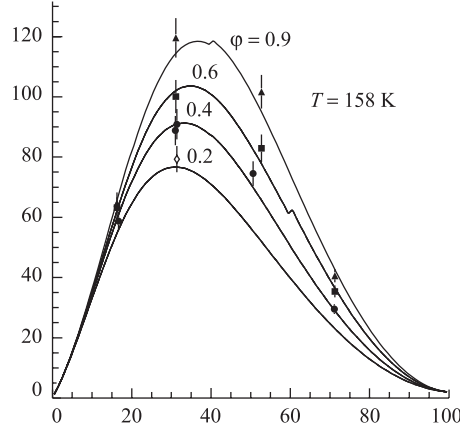

Fig. 3. Normalized cycling rates as a function of the tritium concentration for the low-temperature gaseous D/T mixture [4]. Lines are the optimum fit [4]

As is seen from comparison of Figs. 2, 3, λ_c changes with $\lambda_{dt\mu}$. So, if one consider the «effective» cycling rate for the fast stage (λ_c^f), it should be much more higher than for the steady state (λ_c^s).

3

For the steady state the time distribution of fusion neutrons has the one-exponential form

$$dN_n/dt = N_\mu \cdot \epsilon \cdot \Lambda_c \cdot \exp(-\lambda_n t), \qquad \lambda_n = \lambda_0 + w\Lambda_c, \qquad (3)$$

Here $\Lambda_c = \lambda_c \varphi$; ϵ is the neutron detection efficiency; N_μ is the number of muons stopped in the D/T mixture; w is the muon loss in the cycle which is the probability of muon sticking to helium in fusion reactions, mainly in $d + t$ and also, with lower weight, in the accompanied reactions $d + d$ and $t + t$.

The influence of the $dt\mu$-molecule formation by the «hot» $t\mu$ atoms is reflected both in appearance of the initial «spike», fast component (additional to (3)), and in a change of the parameters (amplitude and slope) of the slow, steady state, component of the time spectrum.

The thermalization rate was estimated to be rather high: $\sim 10^9\,\mathrm{s}^{-1}\varphi$. That is why the spike is hardly observed and interpreted for high ($\varphi = 0.1 - 1$) densities. It was clearly registered in experiments with D/T [7] and $H/D/T$ [8] mixtures at low densities $\varphi \simeq 0.01$.

Knowledge of the parameters of the fast (f) and slow (s) components of the neutron time spectrum allows the extraction of the «pure» lower state cycling rate that is necessary for the correct comparison of experiment with theory. For the muon catalysis of the $d + d$ reaction this was first made in [9] by solving the appropriate differential equations. In [10] the same was done for the first detected neutrons registered with an efficiency ϵ. The steady-state cycling rate can be expressed as

$$\lambda_s = \lambda_c^s \cdot (1 + \delta), \qquad (4)$$

where δ is the relative correction caused by the epithermal effects. This correction can be estimated as

$$\delta \simeq (\lambda_c^f - \lambda_c^s)/\lambda_d. \qquad (5)$$

Epithermal effects for the muon catalysis of the $d + t$ reaction observed in [7] and [8] has been considered in some papers. The most recent and comprehensive articles on this subject are [11] and [12]. The authors analyzed time spectra of all detected neutrons using the Monte-Carlo programs. Full data on the μ-atom scattering cross sections and $dt\mu$-molecule formation rates ($\lambda_{dt\mu}$) as functions of the $t\mu$-atom energy were used in the calculations. Comparing the experimental time spectra with the ones measured at low density the authors have concluded that:

• theoretical values for the $\lambda_{dt\mu}$ for the epithermal $t\mu$ atoms «seem to be overestimated»;

• corrections to the steady-state cycling rate caused by epithermal $dt\mu$ formation can be as large as 40 %.

4

1. MOTIVATION

To compare correctly the values obtained for $\lambda_{dt\mu}$ with the theoretical predictions one should made necessary corrections to the observed steady-state parameters caused by the ephithermal effects.

Of course, some information has been obtained for the epithermal $dt\mu$ formation from the low-density measurements. However, due to complicated kinetics of the MCF in D/T and especially in $H/D/T$ mixtures it does not seem reliable to use the parameters of the fast stage obtained at low density for analyzing the high-density data. It would be very desirable to obtain these parameters and thus the necessary corrections to the steady-state parameters by using experimental data for real (high density) conditions.

This attempt is made in the present work.

2. METHOD

Systematic study of the MCF process in D/T and $H/D/T$ mixtures is carried out by our group at the Joint Institute of Nuclear Research (JINR) Phasotron. The principal features of our experimental method are the use of liquid and high-density tritium targets (up to $\varphi \simeq 1$) and a high-efficiency neutron detection system [13]. For 14 MeV neutrons from the $d + t$ reaction (1) the efficiency is calculated to be $\epsilon \simeq 30\,\%$ [14] for the optimal geometry with the liquid target of small dimensions. Under the conditions for the high-density and high-temperature gaseous targets this value is $\epsilon = (14\text{--}19)\%$.

For such high values of ϵ the measured time spectra of all detected neutrons (which are usually considered in the MCF study) and of the first detected ones are significantly different. In the one-state consideration (without the fast stage) this difference is manifested only in the changing of the slope of the exponent (3): $w \rightarrow \epsilon + w - \epsilon \cdot w$ [15].

The epithermal effects lead to an increase of the slow-component amplitude due to involving the fast stage after each muon regeneration. For the all detected neutrons this effect does not depend on the detection efficiency. The first detected neutrons are less sensitive to muon regeneration (the less sensitive the higher ϵ). Therefore the change of the slow amplitude for the first detected neutrons should be less than for all detected ones. In this paper we obtain corrections due to thermalization stage by comparing the parameters of the time distributions of all detected neutrons and the first detected ones.

Our consideration will follow the effective scheme of Fig. 4: «fast» and «slow» stages with the «effective» cycling rates λ_c^f, λ_c^s and the transition between them with the rate λ_d. Note that we do not try to obtain information on the fast stage parameters. Our aim is to find the way to correctly extract the low-state parameters from the measured data.
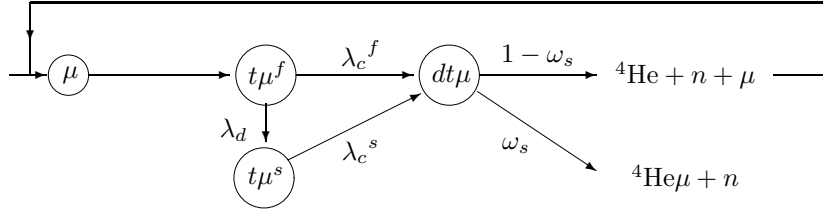
5

Fig. 4. Simplified scheme of the muon catalysis process

The two-states approach allows the use of an analytical method to obtain these effective parameters. A simple system of two differential equations is to be solved for this. In our consideration we treat the MCF rates as a product of the appropriate normalized values and relative density φ.

3. KINETICS

As usual, we shall find the populations of the higher and lower $t\mu$-atom states as functions of time: $n^f(t)$ and $n^s(t)$. The appropriate system of differential equations is

$$dn^f(t)/dt = -(\lambda_0 + \lambda_d + w\lambda_c^f)n^f + (1-w)\lambda_c^s n^s,$$

$$dn^s(t)/dt = -(\lambda_0 + \lambda_c^s)n^s + \lambda_d n^f$$

with the initial conditions $n^f(t=0) = 1$ and $n^s(t=0) = 0$.

The solutions are found in the form

$$n^f = a_{11} \cdot \exp(-\gamma_1 t) + a_{12} \cdot \exp(-\gamma_2 t),$$

$$n^s = a_{21} \cdot \exp(-\gamma_1 t) + a_{22} \cdot \exp(-\gamma_2 t).$$

The «observable» time distribution of all detected neutrons is

$$dN_n(t)/dt = \epsilon \cdot (\lambda_c^f n^f + \lambda_c^s n^s) \equiv \epsilon \cdot (A_f \cdot \exp(-\gamma_f t) + A_s \cdot \exp(-\gamma_s t)), \quad (6)$$

where $A_f = \lambda_c^f \cdot a_{11} + \lambda_c^s \cdot a_{21}$ and $A_s = \lambda_c^f \cdot a_{12} + \lambda_c^s \cdot a_{22}$ are the amplitudes of the fast and slow components, $\gamma_f = \gamma_1$ and $\gamma_s = \gamma_2$ are their slopes.

Exact solution of the system of differential equations gives that the exponents slopes are

$$2\gamma_{1,2} = 2\lambda_0 + \lambda_d + w\lambda_c^f + \lambda_c^s \pm \sqrt{(\lambda_d + w\lambda_c^f + \lambda_c^s)^2 - 4w\lambda_c^s(\lambda_d + \lambda_c^f)},$$

6

and the amplitudes are

$$a_{11} = (\gamma_2 - \lambda_0 - \lambda_d - w\lambda_c^f)/(\gamma_2 - \gamma_1), \quad a_{12} = 1 - a_{11},$$
$$a_{22} = -\lambda_d/(\gamma_2 - \gamma_1), \quad a_{21} = -a_{22}.$$

Due to smallness of w the slow-component slope for all detected neutrons is

$$\gamma_s \simeq \lambda_0 + w\lambda_c^s \frac{\lambda_d + \lambda_c^f}{\lambda_d + w\lambda_c^f + \lambda_c^s} \ .$$

The time distribution of the the first detected neutrons has the same form (6) but with different amplitudes and slopes. To transfer from all detected neutrons to the first detected ones one should make the replacement $w \rightarrow \alpha \equiv \epsilon + w - \epsilon w$ [15] in all formulae.

4. CALCULATIONS

The parameters of the neutron time spectra (amplitudes and slopes of the slow components) were calculated with the use of the formulae of the previous section. Obviously, the effective factor to estimate the cycling rate corrections is the ratio λ_c^f/λ_d. Therefore, we fixed the thermalization rate and the low-state cycling rate and varied the high-state cycling rate. For demonstration we chose the values $\lambda_d \simeq 300\,\mu\mathrm{s}^{-1}$ and $\lambda_c^s \simeq 30\,\mu\mathrm{s}^{-1}$. In Table 1 the calculation results are presented for the parameters

$$\lambda^d = 300\,\mu\mathrm{s}^{-1},\ \lambda_c^s = 30\,\mu\mathrm{s}^{-1},\ w = 0.005,\ \epsilon = 0.3. \tag{7}$$

Table 1. Calculated parameters of the neutron time distributions (6). Parameters (7) were used in the calculations

| Parameter	$\lambda_c^f = 30\,\mu\mathrm{s}^{-1}$ (one state)			
	All detected neutrons		First detected neutrons	
	Exact solution ($\alpha = w = 0.005$)	Monte Carlo	Exact solution ($\alpha = 0.3035$)	Monte Carlo
$\gamma_s,\ \mu\mathrm{s}^{-1}$	0.605	0.606(2)	9.605	9.55(9)
A_s	30.0	30.1(8)	30.0	31.1(5)
	$\lambda_c^f = 300\,\mu\mathrm{s}^{-1}$ (two states)			
	All detected neutrons		First detected neutrons	
	Exact solution ($\alpha = w = 0.005$)	Monte Carlo	Exact solution ($\alpha = 0.3035$)	Monte Carlo
$\gamma_s,\ \mu\mathrm{s}^{-1}$	0.727	0.729(2)	13.9	14.1(2)
A_s	54.1	53.7(1.1)	35.5	36.7(6)
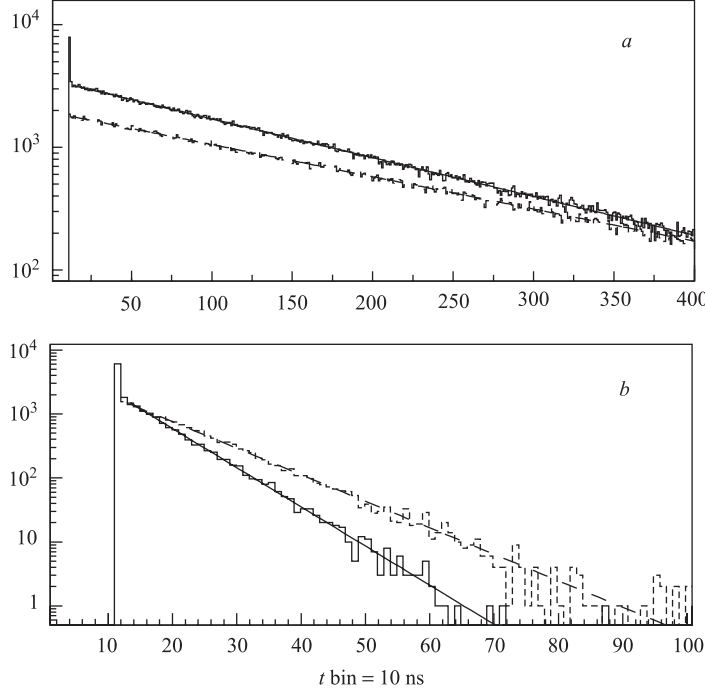
Fig. 5. Time spectra of all detected neutrons (a) and the first detected ones (b) calculated by the Monte-Carlo method with values (7). Dashed-line histograms correspond to the one-state approximation ($\lambda_c^f = \lambda_c^s = 30\,\mu s^{-1}$), solid-line histograms were created with taking into account the fast transition processes ($\lambda_c^f = 300\,\mu s^{-1}$). Lines are the appropriate fit

For the fast state cycling rate we put $\lambda_c^f = 300\,\mu s^{-1}$ and $\lambda_c^f = \lambda_c^s = 30\,\mu s^{-1}$ (one-state approximation).

The time distributions of all detected neutrons and the first detected ones were calculated by the Monte-Carlo method. The scheme of Fig. 4 was used as a basis for the program, the values (7) were put in it. The simulated spectra are shown in Fig. 5. Results of the fit of the simulated distributions are placed in Table 1. As is seen, there is a good agreement between them and the ones obtained by the exact formulae. It is clearly seen from Fig. 5 how the transition process is reflected in the neutron time distributions: a spike arises and the slow component is modified. One can see that the amplitude of the slow component for the first detected neutrons changes only slightly. To know how this effect depends on the «fast» cycling rate and on the neutron detection efficiency the calculations were made with different magnitudes of these values. The results are presented in Fig. 6.
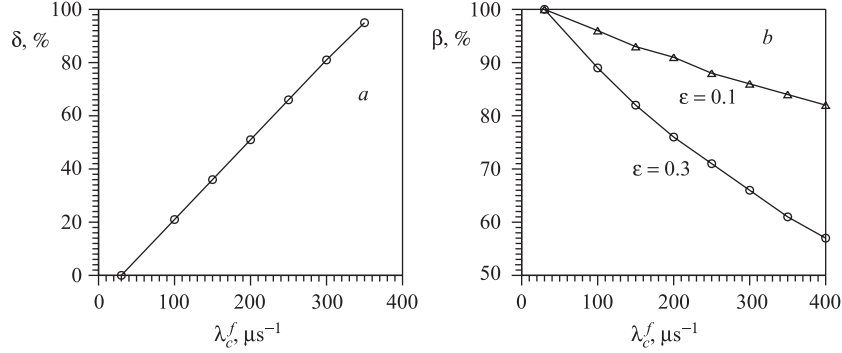
8

Fig. 6. a) The dependence of the value $\delta \equiv (A_s^{\mathrm{all}} - \lambda_c^s)/\lambda_c^f$ on λ_c^f. Calculations were made for $\lambda_d = 300\,\mu s^{-1}$, $\lambda_c^s = 30\,\mu s^{-1}$, $\epsilon = 0.3$. b) The dependence of the value $\beta \equiv A_s^{\mathrm{first}}/A_s^{\mathrm{all}}$ on λ_c^f. Calculations were made for $\lambda_d = 300\,\mu s^{-1}$, $\lambda_c^s = 30\,\mu s^{-1}$

In Fig. 6, a the relative change of the amplitude A_s^{all} for all detected neutrons is given as a function of high state cycling rate. At $\lambda_c^f = \lambda_d$ this change is $\simeq 80\%$. As follows from the data of Fig. 6, b, the ratio of the slow-component amplitudes of the first neutrons to the one of all neutrons strongly depends on the detection efficiency. Hence it is very important to provide as high ϵ as possible.

5. EXPERIMENTAL ESTIMATIONS

The results of the above consideration were applied to an analysis of the experimental data measured with the D/T mixture.

5.1. Choice of the Experimental Conditions. Among many measurements with the D/T mixture made by us in a wide range of φ, C_t and T [4] we chose the ones where, in our opinion, the epithermal effects are manifested most effectively. The main factors are low density and temperature ($T \leq 300$ K) at which thermalized $t\mu$ atoms form $dt\mu$ only on D_2 molecules, and the appropriate rate is relatively small providing small value λ_c^s (see Fig. 2).

The condition with high C_t is the best case to observe the epithermal peak due to the following factors:

• the deceleration rate λ_d is relatively small inasmuch as the scattering cross section $\sigma_{t\mu+t}$ is few times smaller than $\sigma_{t\mu+d}$ [16];

• the cycling rate λ_c^s is small due to the low concentration of D_2 molecules providing a low «base» for the peak.

Decrease of C_t has as a consequence two factors operating in two opposite directions. On the one hand, the deceleration rate increases with decreasing C_t.

9

On the other hand, λ_c^f increases with increasing $C_{D_2} + C_{DT}$, and λ_c^s increases with increasing C_{D_2}. Both factors, compensating for each other, can keep the essential manifestation of epithermal effects. That is why the conditions with different C_t are of interest too.

The parameters of the exposures selected for the analysis are presented in Table 2. Concentrations of molecules determining the MCF intensity in the fast stage (D_2 and DT) and in the slow one (practically only D_2) are also indicated in the Table. It seems that the $dt\mu - t$ resonance is more effective as it is placed at lower $t\mu$ energies. Finally, the measured values of the steady-state cycling rates (λ_c^{exp}) for all detected neutrons (related to $\varphi = 1$) are also shown as presenting the base for the epithermal peak.

In the first experiment with the liquid D/T mixture [13] we had the relative high detection efficiency $\epsilon \simeq 30\,\%$. Unfortunately, in the measurements with the gaseous D/T mixture [4] we could not keep this high efficiency because of the use of high-density, high-temperature targets required «expansion» of the experimental geometry, which caused the essential decrease of ϵ. Of course, it means a decrease of the sensitivity of the method.

Table 2. Parameters of the experimental exposures included in the consideration

T, K	ϵ	φ, LHD	C_t	C_{D_2}	$C_{D_2} + C_{DT}$	λ_s^{exp}, $\mu\mathrm{s}^{-1}$	β^{exp}	$Y_{\mathrm{fast}}^{\mathrm{exp}}$
		0.437	0.31	0.48	0.90	88.7	0.943 ± 0.013	
45, 158	0.139	0.440	0.51	0.24	0.74	73.8	0.936 ± 0.012	
		0.437	0.71	0.08	0.50	30.1	0.940 ± 0.013	0.21 ± 0.04
		0.411	0.31	0.48	0.90	96.0	0.942 ± 0.019	
300	0.194	0.409	0.48	0.27	0.77	89.3	0.896 ± 0.016	
		0.411	0.69	0.10	0.52	50.3	0.895 ± 0.016	0.20 ± 0.05

Time distributions of the first detected neutrons measured with the D/T mixture at $\varphi = 0.4$, $T = 160$ K and $C_t = 70$, 50, 30 % are presented in Fig. 7. The background was subtracted by using the results of the measurements with an empty target. Other spectra taken into consideration ($T = 45$, 300 K) have a similar character for each C_t.

A specific feature of our method is the use of flash ADC to measure the ND charge as a function of time [13]. The strobe pulse frequency was 100 Mc/s which was inadequate to clearly resolve the fast ($\sim 1\,\mathrm{ns}$) process. In addition, the ND signal has finite duration time 30 ns. Both factors result in diffusion of the initial part (time zero region) of the neutron time spectrum. That is why the spike is manifested in the experiment much more weakly as compared with «event mode» distributions (approximately in the ratio $\lambda_d\varphi/20\,\mathrm{ns}$). As follows
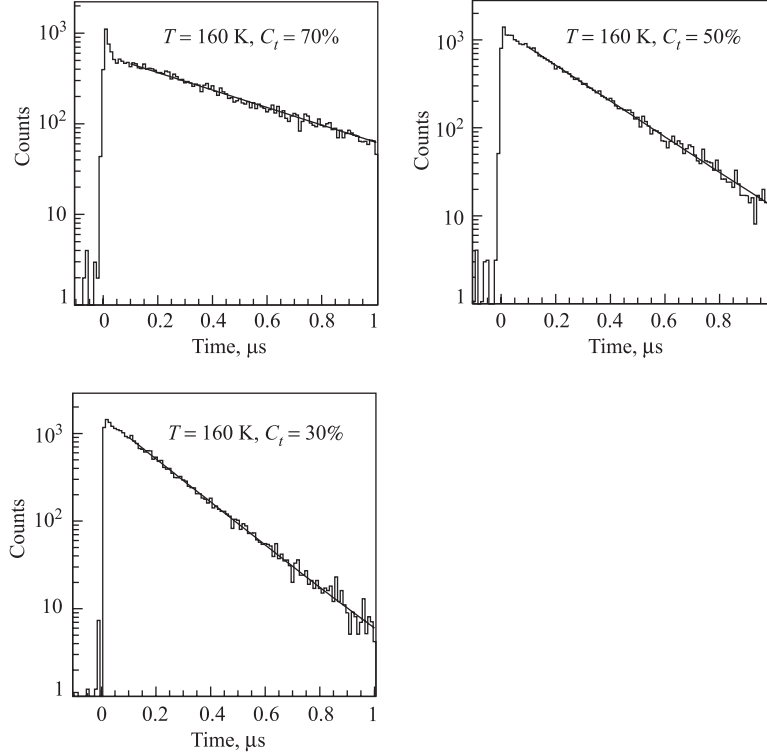
Fig. 7. Time spectra of the first detected neutrons measured in exposures with the D/T mixture at $\varphi = 0.4$, $T = 160$ K and $C_t = 0.7, 0.5, 0.3$

from Fig. 7, the initial peak manifests itself clearly only for the highest tritium concentration $C_t = 0.7$. It may be due to the lowest «base» of the steady state.

5.2. Analysis. In the course of the analysis we fitted the time distribution of all detected neutrons and the first detected ones for the selected conditions (Table 2) to determine the amplitudes of their slow components (steady state) A_s^{all}, A_s^{first} and their ratio β. This was made for all exposures indicated in Table 2. As the data obtained for each C_t were close to each other for $T = 45$, 158 K, they were combined. Averaged results are presented in Table 2 as well as the ones for $T = 300$ K.

Two conclusions can be drawn from the consideration of these data:

• closeness of the values of β for the conditions where λ_c^s changes by several-fold can mean that $\lambda_c^s/\lambda_c^f \ll 1$;

• closeness of β to unity can evidence that $\lambda_c^f \ll \lambda_d$.

11

At the next stage of our treatment we determined the relative corrections δ to the steady-state cycling rate in accordance with the mathematics considered in Sec. 3. Solving the appropriate differential equations with different values λ_c^s, λ_c^f and λ_d, we try to reach the experimental values for $\lambda_s^{\exp}$ and $\beta^{\exp}$ given in Table 2. The calculated optimum values are presented in Table 3. (As our treatment had an estimation character, we did not try to get exact coincidence with experiment.) Thus we got the calculated values close to the «observable» values of the slopes and amplitudes for both components of spectrum (5). So, we could determine not only δ but also the expected yield of the fast component (Y_{fast}).

The following factors are noteworthy.

1. For estimation of λ_d we took into account both the experimental data [7] and the calculated values for the scattering cross sections $\sigma_{t\mu+t}$ and $\sigma_{t\mu+d}$ [16].

2. The input values for λ_c^f were taken to depend on the molecular concentrations C_{D_2} and C_{DT}.

3. The character of the resonances for $T = 300$ K essentially differs from the ones for lower temperatures. This is manifested in their broadening as their height decreases. It means, on the one hand, that $t\mu$ atoms should spend more time to pass the resonances, that is λ_d decreases. On the other hand, it leads to a decrease of the effective value λ_c^f.

Note that the range of the acceptable values for λ_d and λ_c^f may be rather wide, but the stability in λ_s is good enough (5–10 %).

We stress once more that we did not try interpret the parameters of the fast component of the neutron time spectra, we take an interest only in corrections δ to the steady-state cycling rate. As can be seen from Table 3, the corrections to the steady-state cycling rate amount to $\simeq 20\,\%$. We could estimate the experimental value of Y_{fast} only for $C_t = 0.7$ where the steady-state «base» is relatively small. As can be seen from comparison of the data placed in Tables 2, 3, the experimental and calculated values are in satisfactory agreement.

Table 3. The results of the analysis

T, K	C_t	β	λ_c^s, μs^{-1}	λ_s, μs^{-1}	δ	Y_{fast}
	0.31	0.938	72	89.0	0.23	0.22
45, 158	0.51	0.943	60	73.3	0.22	0.21
	0.71	0.950	25	29.9	0.19	0.19
	0.31	0.915	75	96.0	0.28	0.24
300	0.48	0.908	69	89.3	0.28	0.25
	0.69	0.911	40	50.8	0.26	0.24

Of course, our results are obtained in a rather rough model in which the complicated kinetics of the epithermal stage is characterized by only two values: λ_c^f
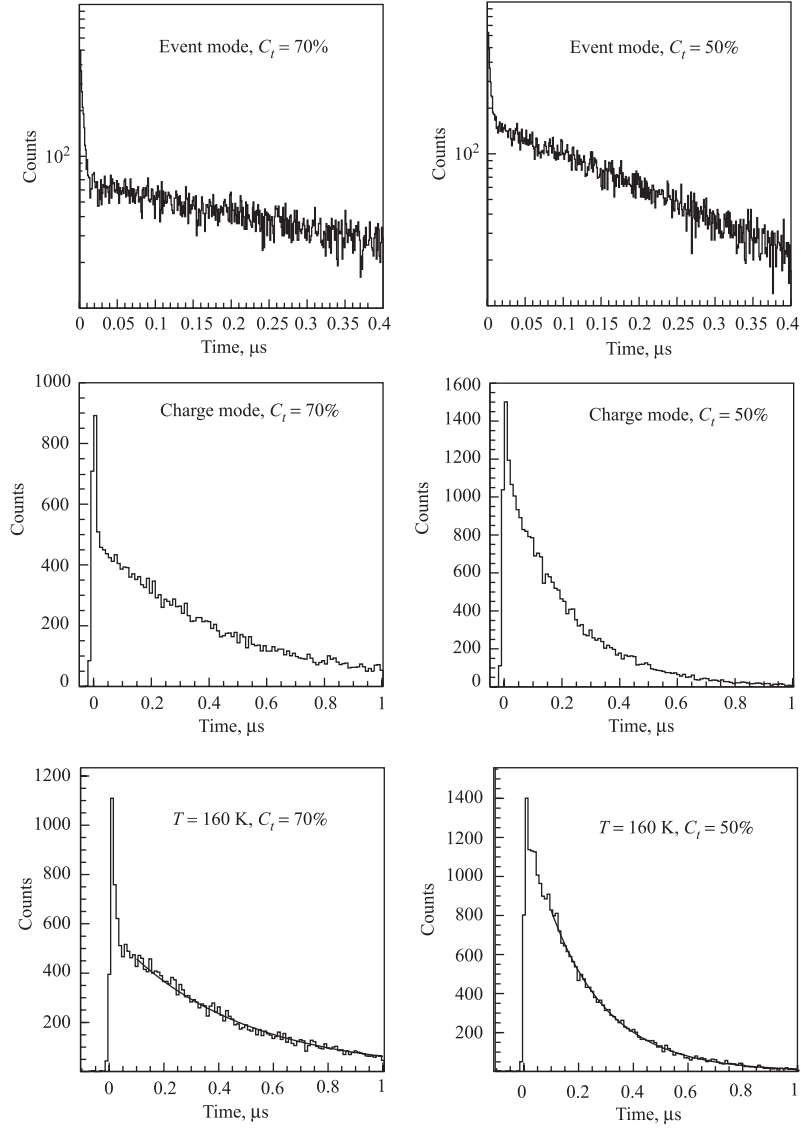
Fig. 8. Time spectra of the first detected neutrons simulated for the optimum analysis parameters for T = 160 K and C_t = 0.7, 0.5 in the «event» (top) and «charge» (middle) modes. For comparison the respective experimental spectra are given (bottom)

and λ_d. That is why it would be important to perform an additional, independent check. First of all, one should try to explain the parameters of the epithermal

13

peak for $C_t = 0.7$ and their evolution for lower C_t. For this aim we made the Monte Carlo calculations of the time spectra of the first detected neutrons with the optimum parameters for $T = 160$ K and $C_t = 0.7$, 0.5. The calculations were performed in two modes. In the first mode («event») the «physical» neutron time spectrum was simulated. The distribution of the number of neutrons in time was simulated for the real values of ϵ and w. In the second («charge») mode the real shape of the ND signals, their amplitude distribution and registration on flash ADC were taken into account. All these spectra are shown in Fig. 8. For comparison the corresponding experimental spectra are also given in the same picture. As is seen, they are rather similar to the simulated ones.

As follows from Table 3, the corrections to the steady-state cycling rate for all detected neutrons (considered by all authors to determine MCF parameters) were estimated to be $\delta = 20$–$25\,\%$. The uncertainty in it is defined by the following factors.

1. The statistical error in β determined by a fit accuracy: $14\,\%$ for the combined data at $T = 45, 158$ K and $18\,\%$ for $T = 300$ K.

2. The uncertainty in the numerical solution for δ: 5–$10\,\%$.

3. Some ambiguity in the ratio of detection efficiencies for all detected neutrons and the first detected ones: 10–$15\,\%$.

Combining all these factors we obtained

$$\delta = 0.21 \pm 0.05 \quad (\varphi = 0.4,\ T = 45, 160\,\mathrm{K},\ C_t = 0.3 \div 0.7),$$

$$\delta = 0.24 \pm 0.06 \quad (\varphi = 0.4,\ T = 300\,\mathrm{K},\ C_t = 0.3 \div 0.7).$$

As can be seen, the corrections in λ_c obtain by us for low φ, T are approximately the same for different tritium concentrations and temperatures. It follows from the analysis of dependences $\lambda_c(C_t)$ with the corrected values λ_c, the real values $\lambda_{dt\mu}$ turned out to be $\simeq 20\,\%$ less than the measured ones. It should be taken into account for correct comparison with theory. For higher density and temperature the corrections should decrease due to the sharp increase of the $dt\mu$-molecule formation rate by thermalized $t\mu$ atoms.

CONCLUSION

Presence of the clear peak (spike) in the neutron time spectra measured by us in exposures with a high-density D/T mixture gives confidence that the corrections to the cycling rate caused by the epithermal effects can be significant. In the present work a method is suggested for interpretation of the steady-state parameters. It was applied to our measurements with D/T carried out with a low-density and low-temperature D/T mixture.

14

REFERENCES

1. *Vesman E.* // Pis'ma Zh. Eksp. Teor. Fiz. 1967. V. 5. P. 113; Sov. Phys. JETP Lett. 1967. V. 5. P. 91.

2. *Faifman M. P., Menshikov L. I., Strizh T. A.* // Muon Catalyzed Fusion. 1989. V. 4. P. 1;
   Faifman M. P., Ponomarev L. I. // Phys. Lett. B. 1991. V. 265. P. 201.

3. *Menshikov L. I., Ponomarev L. I.* // Phys. Lett. B. 1986. V. 167. P. 141.

4. *Bom V. R. et al.* JINR Preprint E15-2004-132. Dubna, 2004; JETP 2005 (in press).

5. *Jones S. E. et al.* // Phys. Rev. Lett. 1983. V. 51. P. 1757; Phys. Rev. Lett. 1986. V. 56. P. 588.

6. *Ackerbauer P. et al.* // Nucl. Phys. A. 1999. V. 652. P. 311.

7. *Breunlich W. H. et al.* // Phys. Rev. Lett. 1984. V. 53. P. 1137; Muon Catalyzed Fusion. 1987. V. 1. P. 67.

8. *Case T. et al.* // Muon Catalyzed Fusion. 1990. V. 5/6. P. 327.

9. *Menshikov L. I. et al.* // Zh. Exp. Teor. Phys. 1987. V. 92. P. 1173; Sov. Phys. JETP. 1987. V. 65. P. 656.

10. *Filchenkov V. V.* JINR Comunication E1-89-57. Dubna, 1989.

11. *Ackerbauer P. et al.* // Nucl. Phys. A. 1999. V. 652. P. 311.

12. *Jeiltler M. et al.* // Phys. Rev. A. 1995. V. 51. P. 2881.

13. *Averin Yu. P. et al.* // Hyp. Int. 1999. V. 118. P. 111.

14. *Bom V. R., Filchenkov V. V.* // Hyp. Int. 1999. V. 119. P. 365.

15. *Filchenkov V. V., Somov L. N., Zinov V. G.* // Nucl. Instr. Meth. 1984. V. 228. P. 174.

16. *Adamchak A. et al.* // Atomic Data and Nuclear Data Tables. 1996. V. 62. P. 255.

Корректор *Т. Е. Попеко*